Solar Energy 144 (2017) 40–48

Contents lists available at ScienceDirect

Solar Energy

journal homepage: www.elsevier.com/locate/solener

On the determination of atmospheric longwave irradiance under all-sky conditions

Mengying Li, Yuanjie Jiang, Carlos F.M. Coimbra *

Department of Mechanical and Aerospace Engineering, Jacobs School of Engineering, Center of Excellence in Renewable Resource Integration and Center for Energy Research, University of California in San Diego, 9500 Gilman Drive, La Jolla, CA 92093, USA

ARTICLE INFO

Article history:
Received 23 June 2016
Received in revised form 24 December 2016
Accepted 3 January 2017

Keywords:
Effective sky emissivity
Effective sky temperature
Downward longwave irradiance
Parametric modeling

ABSTRACT

In this work we review and recalibrate existing models, and present a novel comprehensive model for estimation of the downward atmospheric longwave (LW) radiation for clear and cloudy sky conditions. LW radiation is an essential component of thermal balances in the atmosphere, playing also a substantial role in the design and operation of solar power plants. Unlike solar irradiance, LW irradiance is not measured routinely by meteorological or solar irradiance sensor networks. In most cases, it must be calculated indirectly from meteorological variables using simple parametric models. Under clear skies, fifteen parametric models for calculating LW irradiance are compared and recalibrated. All models achieve higher accuracy after grid search recalibration, and we show that many of the previously proposed LW models collapse into only a few different families of models. A recalibrated Brunt-family model is recommended for future use due to its simplicity and high accuracy (rRMSE = 4.37%). To account for the difference in nighttime and daytime clear-sky emissivities, nighttime and daytime Brunt-type models are proposed. Under all sky conditions, the information of clouds is represented by cloud cover fraction (CF) or cloud modification factor (CMF, available only during daytime). Three parametric models proposed in the bibliography are compared and calibrated, and a new model is proposed to account for the alternation of vertical atmosphere profile by clouds. The proposed all-sky model has 3.8–31.8% lower RMSEs than the other three recalibrated models. If GHI irradiance measurements are available, using CMF as a parameter yields 7.5% lower RMSEs than using CF. For different applications that require LW information during daytime and/or nighttime, coefficients of the proposed models are corrected for diurnal and nocturnal use.

1. Introduction

The downward atmospheric longwave irradiance flux (LW, W/m^2) is an essential component of radiative balance for solar power plants and is of great importance in meteorological and climatic studies, including the forecast of nocturnal temperature variation and cloudiness. It also plays a critical role in the design of radiant cooling systems, as well as in the modeling of weather and climate variability (Alados et al., 2012; Carmona et al., 2014), and on the determination of selective optical properties for photovoltaic panels, photovoltaic-thermal collectors, solar thermoelectricity parabolic disks, etc. (Eicker and Dalibard, 2011; Zaversky et al., 2013).

The downward longwave atmospheric irradiance can be measured directly by pyrgeometers. However, pyrgeometers are not standard irradiance equipment in most weather stations because pyrgeometers are relatively expensive and require extensive calibration and adjustments to exclude the LW radiation emitted by surrounding obstacles, buildings and vegetation. Spectral (line-by-line) calculations considering the interactions of LW irradiance with atmospheric molecules (such as H_2O, CO_2 and O_3), aerosols and clouds yield reasonable estimates of LW for global calculations, but line-by-line calculations are generally too complex for meteorological or engineering use.

A simple approach to estimate LW relies on parametric modeling of meteorological variables measured routinely at the surface level, such as screening level air temperature and relative humidity. The parametric models imply specific assumptions regarding the vertical structure of the atmosphere (Brunt, 1932; Brutsaert, 1975; Ruckstuhl et al., 1984; Maghrabi and Clay, 2011). These assumptions are either explicit (Brutsaert, 1975), or implicitly included in the parametric models by locally fitting coefficients (Berdahl and Fromberg, 1982; Tang et al., 2004; Ruckstuhl et al.,

* Corresponding author.
E-mail address: ccoimbra@ucsd.edu (C.F.M. Coimbra).

http://dx.doi.org/10.1016/j.solener.2017.01.006
0038-092X/

1984; Bilbao and De Miguel, 2007; Maghrabi and Clay, 2011; Carmona et al., 2014).

In this work we review a large number of previous models for determining the downward atmospheric longwave (LW) radiation at the ground level, and propose a novel model for all sky conditions (diurnal and nocturnal, clear or cloudy skies). Section 2 outlines some of the background concepts needed to interpret the dataset and clear sky models used in this work, which are described in Section 3 and in Appendix A. Section 4 discusses and re-calibrates previously proposed models for clear sky conditions, and selects the most accurate model family to be used as a basis for the development of an all-sky condition model, which is evaluated against independent data sets. Conclusions from this work are presented in Section 6.

2. Background

For longwave atmospheric irradiance (4–100 μm), the background atmosphere can be considered as a gray body, and the LW irradiance is approximated as a fraction of a fictional blackbody emissive power evaluated at the surface level air temperature (Mills and Coimbra, 2015). This fraction is called the effective sky emissivity ε_{sky} and is expressed as,

$$\varepsilon_{sky} = \frac{\mathrm{LW}}{\sigma T_a^4} \tag{1}$$

where $\sigma = 5.6697 \times 10_{-8}\ \mathrm{W/m^2\,K^4}$ is the Stefan-Boltzmann constant (Mills and Coimbra, 2015) and T_a (K) is the air temperature at the surface level. This balance can be used to define an effective sky temperature T_{sky} (K) by approximating the sky as a blackbody,

$$\mathrm{LW} = \sigma T_{\mathrm{sky}}^4 \tag{2}$$

Compare Eqs. (1) and (2), the relationship between T_{sky} and $\varepsilon_{\mathrm{sky}}$ is,

$$T_{\mathrm{sky}} = \varepsilon_{\mathrm{sky}}^{1/4} T_a \tag{3}$$

Since $\varepsilon_{\mathrm{sky}}$ ranges from 0 to 1, the effective sky temperature is lower than the surface level air temperature (Mills and Coimbra, 2015).

In the parametric modeling, the clear-sky effective emissivity of the atmosphere can be expressed as a function of screening level air temperature T_a (K), relative humidity ϕ (%) and/or other meteorological variables, including screening level partial pressure of water vapor P_w (Pa), dew point temperature T_d (K) and moisture content d (g/(kg dry air)),

$$\varepsilon_{\mathrm{sky,c}} = f(T_a, \phi, P_w, T_d, d) \tag{4}$$

The partial pressure of water vapor P_w (Pa) and dew point temperature T_d (K) can be expressed as a function of T_a and ϕ by the Magus expressions (Alduchov and Eskridge, 1996),

$$P_w = 610.94\left(\frac{\phi}{100}\right)\exp\left(\frac{17.625(T_a - 273.15)}{T_a - 30.11}\right) \tag{5}$$

$$T_d = \frac{243.04\ln(P_w/610.94)}{17.625 - \ln(P_w/610.94)} + 273.15. \tag{6}$$

And the moisture content d (kg/(kg dry air)) can be expressed as,

$$d = \frac{P_w}{P_a - P_w}\frac{R_a}{R_w} = \frac{0.622P_w}{P_a - P_w}. \tag{7}$$

where P_a is the air pressure (Pa). In Section 4 of this work, fifteen different forms of Eq. (4) are compared and calibrated using measurements from seven stations across the contiguous United States, and the most accurate formula is proposed.

The presence of clouds substantially modifies the LW because the radiation emitted by water vapor and other gases in the lower atmosphere is supplemented by the emission from clouds. Therefore, under cloudy conditions, the effective sky emissivity is higher compared to clear-sky value. Parametric models can also be used to estimate all-sky condition LW with the consideration of cloud contribution,

$$\mathrm{LW} = f(\mathrm{LW}_c, \mathrm{CF}, \mathrm{CMF}) \tag{8}$$

where LW_c ($\mathrm{W/m^2}$) is the corresponding clear-sky LW, CF (%) is the cloud cover fraction in the sky dome and CMF is a cloud modification factor,

$$\mathrm{CMF} = 1 - \frac{\mathrm{GHI}}{\mathrm{GHI}_c} \tag{9}$$

where GHI ($\mathrm{W/m^2}$) is the global horizontal solar radiation and GHI_c ($\mathrm{W/m^2}$) is the clear-sky GHI. Note that CMF only has values during the daytime. In Section 5, three different forms of Eq. (8) are compared and calibrated, and a new model is proposed to achieve higher accuracy.

Therefore, we propose and validate a new parametric modeling of LW for clear- and all-sky conditions applicable to both daytime and nighttime. We validate the model with data from seven stations over the contiguous United States, for which cloud cover fraction data is available in nearby weather stations. A detailed description of the dataset is presented in Section 3.

3. Preparation of dataset

3.1. Observational data

The comparison and calibration of parametric models in Sections 4 and 5 are performed and validated using the radiation and meteorological measurements from the SURFRAD (Surface Radiation Budget Network) and ASOS (Automated Surface Observing System) operated by NOAA (National Oceanic and Atmospheric Administration). Currently seven SURFRAD stations are operating in climatologically diverse regions over the contiguous United States as shown in Fig. 1 (National Oceanic and Atmospheric Administration, 2015). Our fitting and validation datasets include measurements of year 2012 and year 2013 that are collected in all seven stations. Data from years 2014 and 2015 are not selected to avoid the influence of El Niño and La Niña years (Golden Gate Weather Service, 2016).

The seven stations, Bondville (in Illinois), Boulder (in Colorado), Desert Rock (in Nevada), Fort Peck (in Montana), Goodwin Creek (in Mississippi), Penn State University (in Pennsylvania) and Sioux Falls (in South Dakota) represent the climatological diversities, as shown in Table 1. Fort Peck and Sioux Falls have a cold and humid climate with annual averaged temperature and relative humidity around 7.0 °C and 70%. Bondville and Penn State are cool and humid with annual averaged temperature around 11.0 °C and relative humidity around 71%. Boulder has a mild climate with annual averaged temperature and relative humidity of 12.2 °C and 44.7%. Goodwin Creek is warm and humid with annual averaged temperature of 16.8 °C and relative humidity of 71.9%. Desert Rock has a hot and dry climate with annual averaged temperature and relative humidity of 18.8 °C and 27.5%. The seven sites also covers a large altitude span that ranges from 98 m to 1689 m.

The utilized SURFRAD measurements include 1-min averaged downwelling thermal infrared (IR, $\mathrm{W/m^2}$), direct normal solar radiation (DNI, $\mathrm{W/m^2}$), global horizontal solar radiation (GHI, $\mathrm{W/m^2}$), screen level air temperature (T_a, K) and relative humidity of the air (ϕ, %). The Eppley Precision Infrared Radiometer (PIR) measures the downwelling IR from the atmosphere. The spectral range of the

Fig. 1. Locations of the 7 SURFRAD stations used in this work (National Oceanic and Atmospheric Administration, 2015).

Table 1
Annual average values, 25th and 75th percentile of air temperature (T_a), relative humidity (ϕ), downward atmospheric infrared irradiance (IR) of SURFRAD stations during year 2012–2013.

	SURFRAD Stations						
Parameters	Bondville	Boulder	Desert Rock	Fort Peck	Goodwin Creek	Penn State	Sioux Falls
Latitude (°)	40.05	40.13	36.62	48.31	34.25	40.72	43.73
Longtitude (°)	−88.37	−105.24	−116.02	−105.10	−89.87	−77.93	−96.62
Altitude (m)	213	1689	1007	634	98	376	437
Data Sampling Rate (minute)	1	1	1	1	1	1	1
Average T_a (°C)	11.8	12.2	18.8	5.9	16.8	10.7	8.3
25th Percentile of T_a (°C)	2.2	4.3	10.6	−3.8	10.0	2.1	−1.8
75th Percentile of T_a (°C)	20.9	20.6	27.1	16.5	23.9	18.9	19.1
Average ϕ (%)	70.7	44.7	27.5	68.2	71.9	71.0	72.1
25th Percentile of ϕ (%)	58.2	26.2	13.4	52.1	56.8	57.6	58.9
75th Percentile of ϕ (%)	85.6	61.2	35.5	86.4	89.9	87.4	87.9
Average IR (W/m^2)	320.7	290.4	308.0	288.9	349.7	318.0	302.4
25th Percentile of IR (W/m^2)	275.1	248.8	268.6	246.7	307.9	276.4	255.8
75th Percentile of IR (W/m^2)	370.6	331.0	342.7	331.9	396.2	366.6	354.0
	Closest ASOS stations						
	Champaign	Boulder	Desert Rock	Wolf Point INTL	Oxford	State College	Sioux Falls
Latitude (°)	40.04	40.04	36.62	48.09	34.38	40.85	43.58
Longtitude (°)	−88.28	−105.23	−116.03	−105.58	−89.54	−77.85	−96.75
Altitude (m)	163	1612	1009	605	138	378	436
Data Sampling Rate (minute)	60	20	60	60	20	20	60

PIR is 3 μm to 50 μm (National Oceanic and Atmospheric Administration, 2015). The Normal Incidence Pryheliometer (NIP) measures the DNI in the broadband spectural range from 0.28 μm to 3 μm (National Oceanic and Atmospheric Administration, 2015). The Spectrolab SR-75 pyranometer measures the GHI in the same spectral range as the NIP (National Oceanic and Atmospheric Administration, 2015). All irradiance instruments have uncertainties smaller than ±5 W/m^2, and are calibrated annually. The data quality is controlled by NOAA using the methodology outlined for the Baseline Surface Radiation Network, where low quality data are deleted and questionable data are flagged (less than 1% of data). The instruments are calibrated against standards traceable to the World Radiation Center in Davos, Switzerland (National Oceanic and Atmospheric Administration, 2015). Questionable data falling outside of physically possible values were also flagged and deleted from our dataset. Since large amounts of measured data are used in this work, the uncertainty is statistically reduced. Less than 0.5% of the original data has been deleted for this study. The cloud fraction (CF) is obtained from closest ASOS stations (Table 1). ASOS network has over 3000 operational stations over the contiguous United States and its data are publicly available for download from the website of Iowa State University of Science and Technology (Iowa State University of Science and Technology, 2016). The cloud fraction in ASOS is reported in three layers. The amount of cloud is determined by adding the total number of hits in each layer and

computing the ratio of those hits to the total possible. If there is more than one layer, the 'hits' in the first layer are added to the second (and third) to obtain overall coverage (National Oceanic and Atmospheric Administration, 1998). ASOS stations measure20-min or 60-min averaged text-annotated CF information while in this work, the CF is interpreted as numerical values based on Table 2. When CF data are in use, the 1-min averaged SURFRAD data are interpolated to match the timestamp of the CF data by nearest neighbor interpolation.

3.2. Selection of clear-sky periods

For the analysis of clear-sky parametric models, only clear-sky periods are selected. The clear-sky periods are defined as the periods where no cloud presents within the field of view of the radiometers. During the daytime, GHI and DNI time series are used instead of CF data because irradiance measurements are available on-site and are sampled at 1-min intervals. The CF data have an uncertainty of ±0.125, sampled every 20 or 60 min and are retrieved from nearby ASOS stations. An endogenous statistical model which was originally developed by Reno et al. for GHI observations (Reno et al., 2012) is used to select clear-sky periods. This method uses five criteria to compare a period of N GHI measurements to a corresponding clear-sky GHI for the same period. In this work, the clear-sky GHI and DNI values are calculated using clear-sky models adapted from References Kasten and Young (1989), Ineichen and Perez (2002), Ineichen (2006, 2008), and Inman et al. (2015), which are presented in Appendix A.

The time period is deemed 'clear' if threshold values for all the following criteria are met when compared with clear-sky irradiance time series:

1. The difference of mean value of irradiance I and clear-sky irradiance I_c in the time series,

$$\left|\frac{1}{N}\sum_{n=1}^{N} I(t_n) - \frac{1}{N}\sum_{n=1}^{N} I_c(t_n)\right| < \theta_1 \tag{10}$$

2. The difference of max value of I and I_c in the time series,

$$|\max I(t_n) - \max I_c(t_n)| < \theta_2, \quad n \in [1,2,\ldots,N] \tag{11}$$

3. The difference of length of the line connecting the points in the time series (Inman et al., 2015), without the consideration of the length of the time-step,

$$\left|\sum_{n=1}^{N}|s(t_n)| - \sum_{n=1}^{N}|s_c(t_n)|\right| < \theta_3 \tag{12}$$

where slopes $s(t_n) = I(t_n + \Delta t) - I(t_n)$ and $s_c(t_n) = I_c(t_n + \Delta t) - I_c(t_n)$.

4. The difference of maximum deviation from the clear-sky slope,

$$\max|s(t_n) - s_c(t_n)| < \theta_4, \quad n \in [1,2,\ldots,N] \tag{13}$$

5. The difference of the normalized standard deviation of the slope between sequential points,

$$\left|\frac{\sqrt{\frac{1}{N-1}\sum_{n=1}^{N-1}(s(t_n)-\bar{s})^2}}{\frac{1}{N}\sum_{n=1}^{N} I(t_n)} - \frac{\sqrt{\frac{1}{N-1}\sum_{n=1}^{N-1}(s_c(t_n)-\bar{s}_c)^2}}{\frac{1}{N}\sum_{n=1}^{N} I_c(t_n)}\right| < \gamma_5 \tag{14}$$

Specific thresholds for both GHI and DNI are used in this work, resulting in a total of 10 criteria. A 10-min sliding window is employed as suggested by References Reno et al. (2012) and Inman et al. (2015). In this work, a period is classified as clear only if all 10 criteria are met for measured GHI and DNI time series in at least one sliding window around the referred period. The threshold values for GHI and DNI are obtained from Reference Inman et al. (2015) and tabulated in Table 3. The threshold values $\theta_1, \theta_2, \theta_3$ and θ_4 have units of W/m^2 because they represent the differences of irradiance or slope as defined in Eqs. (10)–(13). The threshold value γ_5 is dimensionless because it represents the difference of normalized standard deviation of the slope as defined in Eq. (14).

During the nighttime, a period is denoted as clear if ASOS cloud fraction (CF) is zero during the whole night.

3.3. Measured atmospheric longwave irradiance

In Refs. Bilbao and De Miguel (2007) and Alados et al. (2012) and many others, the measurements from the PIR are used directly as the LW irradiance. However, the Eppley PIR only measures infrared irradiance from 3 μm to 50 μm, which is a subset range of the total LW irradiance. To account for this discrepancy, we calculate the effective sky temperature T_{sky} iteratively using the proper spectral range,

$$\mathrm{IR} = \sigma T_{\mathrm{sky}}^4 F_{\lambda_1-\lambda_2}(T_{\mathrm{sky}}) \tag{15}$$

where IR is the measured infrared flux from PIR and $F_{\lambda_1-\lambda_2}$ is the external fraction of blackbody emission, which is calculated as,

$$F_{\lambda_1-\lambda_2}(T) = \frac{\int_{\lambda_1}^{\lambda_2} E_{b,\lambda}(T)d\lambda}{\int_0^{\infty} E_{b,\lambda}(T)d\lambda} = \frac{\int_{\lambda_1}^{\lambda_2} E_{b,\lambda}(T)d\lambda}{\sigma T^4} \tag{16}$$

where $\lambda_1 = 3$ μm and $\lambda_2 = 50$ μm that match the measurement range of the Eppley PIR. The measured downward atmospheric longwave irradiance is then expressed as,

$$\mathrm{LW}_S = \sigma T_{\mathrm{sky}}^4 \tag{17}$$

3.4. Assessment metrics

Four statistical metrics are implemented to assess the accuracy of the parametric models: mean biased error (MBE), root mean square error (RMSE), relative mean biased error (rMBE) and relative root mean square error (rRMSE).

$$\mathrm{MBE} = \frac{1}{K}\sum_{k=1}^{K}(\mathrm{LW}_{M,k} - \mathrm{LW}_{S,k}) \tag{18}$$

$$\mathrm{RMSE} = \sqrt{\frac{1}{K}\sum_{k=1}^{K}(\mathrm{LW}_{M,k} - \mathrm{LW}_{S,k})^2}, \tag{19}$$

$$\mathrm{rMBE} = \frac{\mathrm{MBE}}{1/K\sum_{k=1}^{K}\mathrm{LW}_{S,k}} \tag{20}$$

$$\mathrm{rRMSE} = \frac{\mathrm{RMSE}}{1/K\sum_{k=1}^{K}\mathrm{LW}_{S,k}} \tag{21}$$

Table 2
Numerical interpretation of ASOS text-annotated cloud fraction (National Oceanic and Atmospheric Administration, 1998).

ASOS text-annotated cloud fraction (CF)	Clear	Few	Scattered	Broken	Overcast
Numerical cloud fraction (CF)	0	0.125	0.375	0.75	1

Table 3
Clear-sky criteria threshold values for GHI and DNI from Inman et al. (2015).

	GHI thresholds	DNI thresholds
θ_1 (W/m^2)	100	200
θ_2 (W/m^2)	100	200
θ_3 (W/m^2)	50	100
θ_4 (W/m^2)	10	15
γ_5	0.01	0.015

where K is the number of data points in the validation dataset, LW_M is the modeled longwave irradiance and LW_S is the measured longwave irradiance (Eq. (17)).

The number of data points used in this work is tabulated in Table 4. The data are randomly selected from the fitting and validation datasets to include measurements from all seasons and all seven SURFRAD stations. The clear-sky data are randomly selected from the dataset when the sky is deemed clear while the all-sky data are randomly selected from the entire dataset.

All the results tabulated in the following Sections 4 and 5 are calculated based on the validation dataset (Table 4) while the plots illustrate only a random subset to improve the readability of the figures.

4. Parametric models for clear-sky conditions

4.1. Calibration of selected models

Since 1910s, researchers have developed several parametric models to quantify the relationship between the clear-sky effective sky emissivity and ground level meteorologic information. The meteorologic information includes the air temperature T_a (K), the relative humidity ϕ (%), water vapor pressure P_w (Pa), dew point temperature T_d (K), integrated water content in a vertical air column w (mm) and moisture content d (g/(kg dry air)).

Selected parametric clear-sky models are presented in chronological order in Table 5. The numerical coefficients in each model were originally fitted using local meteorologic measurements. A grid search method is used to calibrate the coefficients of the parametric models based on our dataset. The grid search method lays the coefficient values on a grid, and each parametric model is evaluated on the fitting dataset using a combination of coefficients at a time. Then the combination of coefficients that results in the smallest RMSE is selected as the calibrated set of coefficients. Clear-sky SURFRAD data collected in year 2012 is used as fitting dataset and data collected in year 2013 is used as a validation dataset to evaluate the performance of original and calibrated models.

4.2. Results and discussions

4.2.1. Calibration increases the accuracy of all models

Fig. 2 presents a comparison between the original and calibrated Brunt model. Both the bias and absolute errors are reduced by the calibration and the reduction applies for all other models. The MBE, RMSE, rMBE and rRMSE of those models in calculating LW before and after the calibrations are presented in Table 6. As shown in Table 6, after the calibration of coefficients, the RMSE of all models improved by 2.8–58.9% and some formulas are substantially better than others. The Swinbank, Idso and Jackson and Ruchstuhl models have errors around twice of that of other models, indicating that these three formulas are not recommended for future use.

Table 4
The number of data points used in this work.

	Fitting dataset (year 2012)	Validation dataset (year 2013)
Daytime clear-sky periods	8287	6912
Nigttime clear-sky periods	8840	7140
All day clear sky periods	17,127	14,052
Daytime all sky condition periods	4719	5403
Nighttime all sky condition periods	4185	4614
All day all sky condition periods	8904	10,017

4.2.2. Different functional forms corresponding to the same model

Even though the parametric models described above have different functional forms and different coefficients as shown in Table 5, most models have nearly identical accuracies after the calibration of their coefficients as shown in Table 6. Further examination of the modeling results show that most of the examined parametric models correspond to only a few independent model families. As shown in Fig. 3, LW_c calculated by calibrated Brunt, Brutsaert, Berdahl and Fromberg, Berdahl and Martin, Prata, Dilley and O'Brien, Niemelä, Iziomon, and Dai and Fang models correspond to the same model family. The models proposed by Idso, Satterlund and Carmona also yield identical values of LW_c after the calibration and they collapse to another model family. The different functional forms relate only to the use of different variables that are not independent from each other. In other words, each model family represents the same model expressed in terms of either mutually dependent or redundant variables. In these cases, the increased complexity of the functional relationships does not yield higher accuracy. Since the calibrated Brunt model has the simplest functional form (only one variable with two coefficients) and remains the most accurate, we recommend its use as the baseline model for further developments.

4.2.3. The nighttime clear sky is more emissive than the daytime

By comparing the effective clear sky emissivity during the nighttime and the daytime, a positive difference is observed, indicating that the clear sky is more emissive during the night. Fig. 4 shows that on average, the nighttime emissivity is around 0.035 higher than the daytime values under the same ground-level partial pressure of water vapor. This behavior is related to the formation of inversion layers during clear nights where the surface temperature is reduced compared with the temperature aloft (Berdahl and Fromberg, 1982). The day and night difference is observed by other studies as well (Berdahl and Fromberg, 1982; Dupont et al., 1984; Alados et al., 2012).

For energy balance applications in solar engineering, the effective emissivity during the daytime is more favorable while for nighttime passive cooling applications, the effective emissivity during the nighttime is more favorable. Therefore, the parametric clear-sky Brunt models for both daytime and nighttime are proposed as,

$$\text{Daytime clear-sky model}: \varepsilon_{\text{sky},c} = 0.598 + 0.057\sqrt{P_w} \quad (22a)$$

$$\text{Nighttime clear-sky model}: \varepsilon_{\text{sky},c} = 0.633 + 0.057\sqrt{P_w} \quad (22b)$$

$$\text{All day clear-sky model}: \varepsilon_{\text{sky},c} = 0.618 + 0.056\sqrt{P_w} \quad (22c)$$

Table 7 presents the modeling errors of time specified Brunt models. Daytime Brunt model has the highest accuracy during the daytime and nighttime Brunt model has the highest accuracy during nighttime. For applications that require both daytime and nighttime LW_c information, the all-sky Brunt model is the most accurate model to use.

Table 5
Parametric models for clear skies.

Model	Year Developed	Variables	Formulation	Original Parameters
Brunt (1932)	1932	P_w (hPa)	$\varepsilon_{sky} = c_1 + c_2\sqrt{P_w}$	$c_1 = 0.52, c_2 = 0.065$
Swinbank (1963)	1963	T_a (K)	$\varepsilon_{sky} = c_1 T_a^{c_2}$	$c_1 = 9.365 \times 10^{-6}, c_2 = 2$
Idso and Jackson (1969)	1969	T_a (K)	$\varepsilon_{sky} = 1 - c_1 \exp[c_2(273 - T_a)^{c_3}]$	$c_1 = 0.261, c_2 = -7.77 \times 10^{-4}, c_3 = 2$
Brutsaert (1975)	1975	P_w (hPa), T_a (K)	$\varepsilon_{sky} = c_1 (P_w/T_a)^{c_2}$	$c_1 = 1.24, c_2 = 1/7$
Satterlund (1979)	1979	P_w (hPa), T_a (K)	$\varepsilon_{sky} = c_1[1 - \exp(-P_w^{T_a/c_2})]$	$c_1 = 1.08, c_2 = 2016$
Idso (1981)	1981	P_w (hPa), T_a (K)	$\varepsilon_{sky} = c_1 + c_2 P_w \exp(c_3/T_a))$	$c_1 = 0.70, c_2 = 5.95 \times 10^{-5}, c_3 = 1500$
Berdahl and Fromberg (1982)	1982	T_d (°C)	$\varepsilon_{sky} = c_1 + c_2 T_d$ (daytime)	$c_1 = 0.727, c_2 = 0.0060$
Berdahl and Martin (1984)	1984	T_d (°C)	$\varepsilon_{sky} = c_1 + c_2(T_d/100) + c_3(T_d/100)^2$	$c_1 = 0.711, c_2 = 0.56, c_3 = 0.73$
Prata (1996)	1996	w (g/cm^2), P_w (hPa), T_a (K)	$\varepsilon_{sky} = 1 - (1 + w)\exp(-\sqrt{(c_1 + c_2 w)}), w = c_3 \frac{P_w}{T_a}$	$c_1 = 1.2, c_2 = 3, c_3 = 46.5$
Dilley and O'brien (1998)	1998	T_a (K), w (kg/m^2)	$\varepsilon_{sky} = \left(c_1 + c_2\left(\frac{T_a}{273.16}\right)^6 + c_3\sqrt{\frac{w}{25}}\right)\Big/\sigma T_a^4, w = 4.65\frac{P_w}{T_a}$	$c_1 = 59.38, c_2 = 113.7, c_3 = 96.96$
Niemelä et al. (2001)	2001	P_w (hPa)	$\varepsilon_{sky} = c_1 + c_2(P_w - c_3)$, if $P_w \geqslant c_3$	$c_1 = 0.72, c_2 = 0.009, c_3 = 2$
			$\varepsilon_{sky} = c_1 - c_2(P_w - c_3)$, if $P_w < c_3$	$c_1 = 0.72, c_2 = 0.076, c_3 = 2$
Iziomon et al. (2003)	2003	P_w (hPa), T_a (K)	$\varepsilon_{sky} = 1 - c_1 \exp\left(\frac{-10P_w}{T_a}\right)$	$c_1 = 0.35$
Ruckstuhl et al. (1984)	2007	w (mm), d (g/kg)	$\varepsilon_{sky} = c_1 w^{c_2}, w = c_3 d - c_4$	$c_1 = 147.8, c_2 = 0.26, c_3 = 2.40, c_4 = 1.60$
Dai and Fang (2014)	2014	P_w (hPa), P_a (hPa)	$\varepsilon_{sky} = (c_1 + c_2 P_w^{c_3})(P_a/1013)^{c_4}$	$c_1 = 0.48, c_2 = 0.17, c_3 = 0.22, c_4 = 0.45$
Carmona et al. (2014)	2014	T_a (K), ϕ (%)	$\varepsilon_{sky} = -c_1 + c_2 T_a + c_3\phi$	$c_1 = 0.34, c_2 = 3.36 \times 10^{-3}, c_3 = 1.94 \times 10^{-3}$

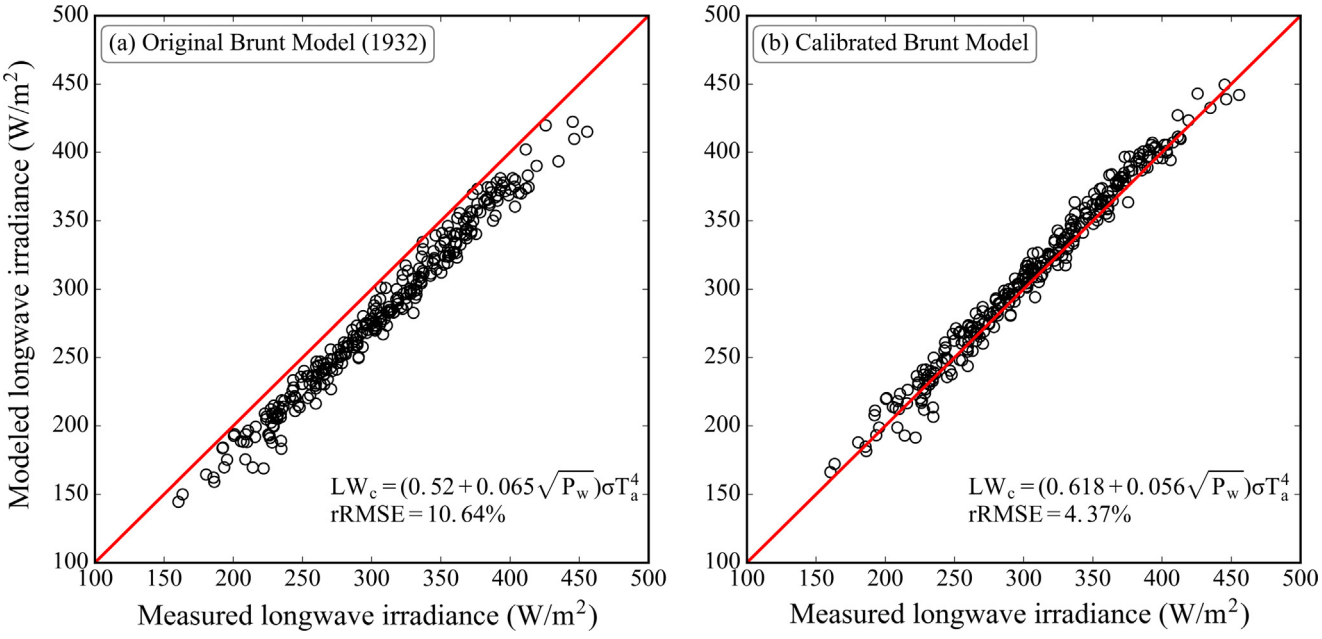

Fig. 2. Modeled LW with respect to measured LW. (a) Original Brunt model; (b) Calibrated Brunt model.

5. Parametric models for all-sky conditions

5.1. Calibration of selected and proposed models

Under all-sky conditions, the downward longwave irradiance is increased by the radiation emission from clouds (liquid water and/or ice). Therefore, the all-sky parametric models need to include cloud information such as cloud cover fraction (CF) or cloud modification factor (CMF). In 1999, Crawford and Duchon (1999) developed a parametric model that accounts for the emission of clouds in the form of,

$$\mathrm{LW} = \mathrm{LW}_c(1 - c_1\mathrm{CF}^{c_2}) + c_3\mathrm{CF}^{c_4}\sigma T_a^4 \tag{23}$$

In the original Crawford and Duchon model, all the four coefficients $c_1 \sim c_4$ are equal to 1. Other parametric models proposed by References Konzelmann et al. (1994) and Duarte et al. (2006) would also collapse to this form with different $c_1 \sim c_4$.

A parametric model for daytime all-sky condition was proposed by Bilbao and De Miguel (2007),

$$\mathrm{LW} = \mathrm{LW}_c(1 + c_1\mathrm{CMF}^{c_2}) \tag{24}$$

where c_1 and c_2 are coefficients regressed from local measurements.

Another model proposed by Alados et al. (2012) has the functional relation

$$\mathrm{LW} = \mathrm{LW}_c(c_1 - c_2(1 - \mathrm{CMF})) \tag{25}$$

where c_1 and c_2 are locally fitted coefficients as well.

To account for the modification of LW due to clouds, we propose a comprehensive new model as shown in Eq. (26) where CMF or CF equals to zero corresponds to clear (cloud free) conditions. The first

Table 6
LW_c modeling errors of original and calibrated clear-sky models.

Model	Original models				Calibrated Parameters	Calibrated models			
	MBE (W/m^2)	RMSE (W/m^2)	rMBE (%)	rRMSE (%)		MBE (W/m^2)	RMSE (W/m^2)	rMBE (%)	rRMSE (%)
Brunt (1932)	29.54	32.24	9.75	10.64	$c_1 = 0.618, c_2 = 0.056$	−0.94	13.24	−0.31	4.37
Swinbank (1963)	3.70	30.30	1.22	10	$c_1 = 9.169 \times 10^{-6}, c_2 = 2$	−2.70	29.45	−0.89	9.72
Idso and Jackson (1969)	9.63	30.51	3.18	10.07	$c_1 = 0.242, c_2 = -1.8 \times 10^{-4}$	−0.52	25.81	−0.17	8.52
Brutsaert (1975)	−18.91	23.69	−6.24	7.82	$c_1 = 1.168, c_2 = 1/9$	−1.94	13.54	−0.64	4.47
Satterlund (1979)	5.42	16.36	1.79	5.4	$c_1 = 1.02, c_2 = 1564.94$	−1.12	14.63	−0.37	4.83
Idso (1981)	5.21	14.03	1.72	4.63	$c_1 = 0.685, c_2 = 3.2 \times 10^{-5}, c_3 = 1699$	−0.39	13.18	−0.13	4.35
Berdahl and Fromberg (1982)	−15.21	20.06	−5.02	6.62	$c_1 = 0.764, c_2 = 5.54 \times 10^{-3}$	−1.00	13.57	−0.33	4.48
Berdahl and Martin (1984)	−18.36	22.42	−6.06	7.4	$c_1 = 0.758, c_2 = 0.521, c_3 = 0.625$	−0.70	13.24	−0.23	4.37
Prata (1996)	−6.91	15.00	−2.28	4.95	$c_1 = 1.02, c_2 = 3.25, c_3 = 52.7$	−1.67	13.15	−0.55	4.34
Dilley and O'brien (1998)	−19.81	24.03	−6.54	7.93	$c_1 = 55.08, c_2 = 125.03, c_3 = 108.83$	−0.33	12.48	−0.11	4.12
Niemelä et al. (2001)	2.85	14.88	0.94	4.91	$c_1 = 0.712, c_2 = 8.7 \times 10^{-3}, c_3 = 1.52$ $c_1 = 0.66, c_2 = -0.0107, c_3 = 1.52$	−1.85	13.82	−0.61	4.56
Iziomon et al. (2003)	−15.91	20.66	−5.25	6.82	$c_1 = 0.33, c_2 = 13.78$	−1.24	13.15	−0.41	4.34
Ruckstuhl et al. (1984)	−42.87	56.62	−14.15	18.69	$c_1 = 184, c_2 = 0.2, c_3 = 3.1, c_4 = 0.5$	4.97	34.87	1.64	11.51
Dai and Fang (2014)	−24.93	28.78	−8.23	9.5	$c_1 = 0.32, c_2 = 0.34, c_3 = 0.16, c_4 = 0.2$	−2.36	13.24	−0.78	4.37
Carmona et al. (2014)	−21.06	25.33	−6.95	8.36	$c_1 = -0.503, c_2 = 4.04 \times 10^{-3}, c_3 = 2.4 \times 10^{-3}$	0.39	13.12	0.13	4.33

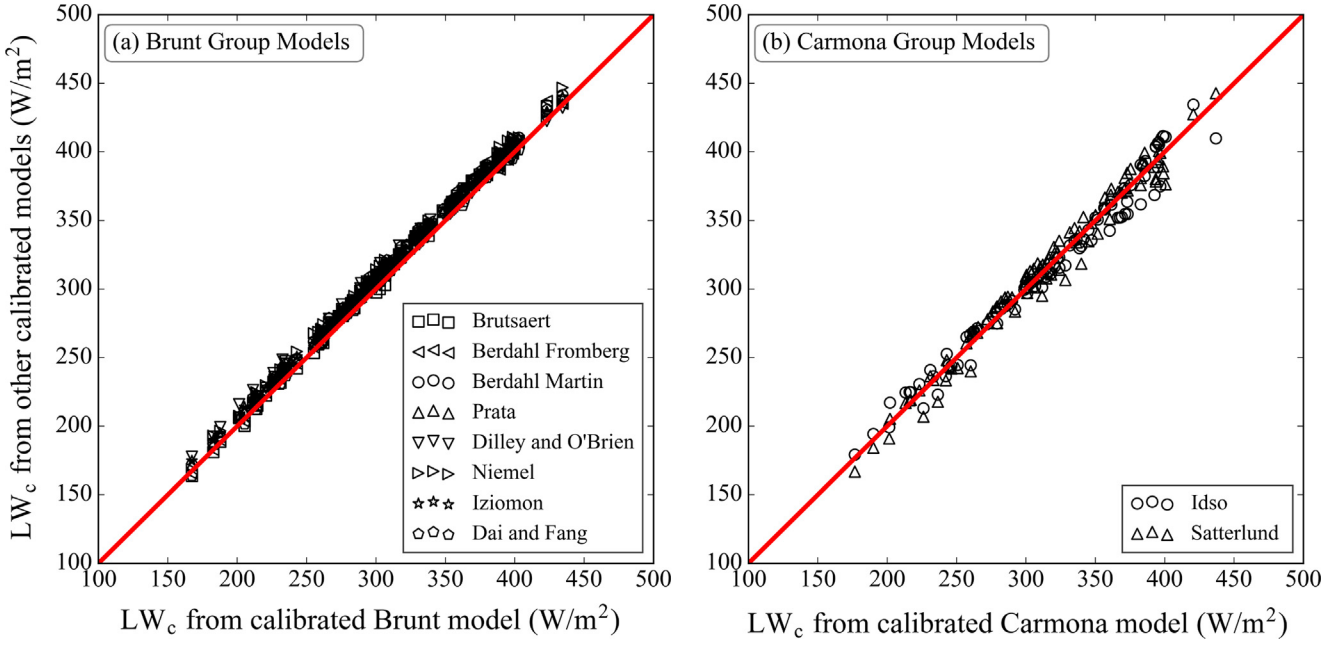

Fig. 3. Comparison of different calibrated clear-sky models (a) The Brunt model group; (b) The Carmona model group.

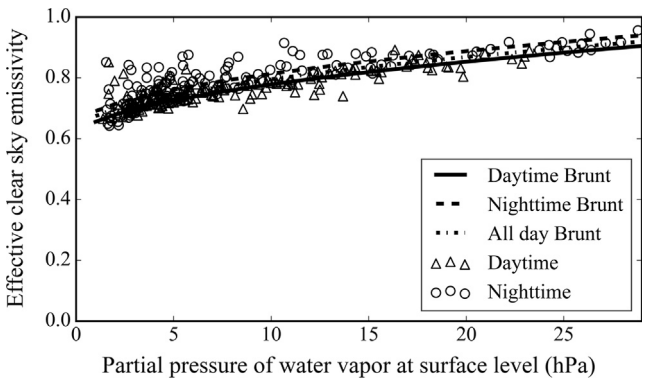

Fig. 4. Comparison of clear sky emissivity during the nighttime and during the daytime.

term on the right-hand side of Eq. (26) accounts for the absorption of LW by clouds and the second term accounts for the emission of LW by clouds. The alteration of vertical atmospheric temperature and relative humidity profile by clouds is represented by using screening level temperature T_a and relative humidity ϕ as parameters in the second right-hand side term of Eq. (26). Although many functional forms are possible for the weighing functions, we opted for a simple linear to power-law scale dependency, which fits well the data.

$$\text{Daytime model}: \quad \mathrm{LW} = \mathrm{LW}_c(1 - c_1\mathrm{CMF}^{c_2}) + c_3\sigma T_a^4 \mathrm{CMF}^{c_4}\phi^{c_5} \tag{26a}$$

$$\text{All day model}: \quad \mathrm{LW} = \mathrm{LW}_c(1 - c_1\mathrm{CF}^{c_2}) + c_3\sigma T_a^4 \mathrm{CF}^{c_4}\phi^{c_5} \tag{26b}$$

The three previously proposed models (Eq. (23)–(25)) with their original coefficients are tested on the validation sets and their coefficients are recalibrated by a grid search method to improve their

Table 7
LW_c modeling errors of time specified Brunt models. Bold values indicate best performance.

	Model	Daytime Brunt, Eq. (22a)	Nighttime Brunt, Eq. (22b)	All-day Brunt, Eq. (22c)
Daytime clear-sky periods	MBE (W/m^2)	−1.99	12.18	4.98
	RMSE (W/m^2)	8.54	15.16	9.86
	rMBE (%)	−0.65	3.95	1.61
	rRMSE (%)	**2.77**	4.91	3.2
Nighttime clear-sky periods	MBE (W/m^2)	−13.19	0.01	−6.68
	RMSE (W/m^2)	19.42	14.57	15.85
	rMBE (%)	−4.43	0.00	−2.24
	rRMSE (%)	6.53	**4.89**	5.33
All day clear-sky periods	MBE (W/m^2)	−7.68	6.00	−0.94
	RMSE (W/m^2)	15.08	14.86	13.25
	rMBE (%)	−2.54	1.98	−0.31
	rRMSE (%)	4.98	4.91	**4.37**

accuracy for comparison. The coefficients of the proposed new models (Eq. (26)) are fitted to the *fitting* dataset and validated against the *validation* dataset.

5.2. Results and discussions

Using the calibrated clear-sky Brunt model (Eq. (22)) to calculate the clear-sky LW_c, the MBE, RMSE, rMBE and rRMSE of all-sky models in modeling LW are presented in Table 8. The accuracies of Carwford and Duchon, Bilbao and Aldos model increase after the calibration of coefficients. During the daytime periods, the proposed all-sky model outperforms the three other models and has 15.3–31.8% lower RMSE. If GHI irradiance measurements are available, using CMF has 7.5% lower RMSE than using CF. During the nighttime, the proposed model (Eq. (26b)) has 1.3% lower RMSE than the calibrated Crawford and Duchon model. During all day periods, the proposed model (Eq. (26b)) has 3.8% lower RMSE than the calibrated Carwford and Duchon model. For different applications that require daytime and/or nighttime LW information, specific values of $c_1 \sim c_5$ of proposed model can be selected from Table 8.

6. Conclusions

Under clear-sky conditions, fifteen parametric models proposed in the bibliography to estimate downward atmospheric longwave irradiance (LW_c) are compared and recalibrated using data collected from 7 climatologically diverse SURFRAD stations over the contiguous United States. All fifteen models achieve 2.8–58.9% smaller errors when their coefficients are recalibrated. After the recalibration, we identify several models as yielding identical values of LW_c, which indicate that they are different expression of the same model, and that the increased complexities of the proposed formulas does not result in higher accuracies. Models that correspond to the recalibrated Brunt model include the ones proposed by References Brutsaert (1975), Berdahl and Fromberg (1982), Berdahl and Martin (1984), Prata (1996), Dilley and O'brien (1998), Niemelä et al. (2001), Iziomon et al. (2003), and Dai and Fang (2014). Another group of models correspond to recalibrated Carmona model, and includes the ones proposed by References Satterlund (1979) and Idso (1981). Since the expression of effective sky emissivity in the Brunt model has only two coefficients and one variable and it achieves high accuracy (rRMSE = 4.37%), the use of recalibrated clear-sky Brunt models is recommended.

Clear night skies has higher effective emissivity than clear days at the same level of surface partial pressure of water vapor, which is observed in this work. The clear nighttime emissivity is larger than the daytime value by 0.035. Therefore, both daytime and nighttime calibrated Brunt-type models are proposed and validated in this study.

Under all sky conditions, the parametric models for calculating LW should consider the radiation emitted from clouds. The information of clouds is represented by simple cloud cover fractions (CF) or cloud modification factors (CMF, only valid during daytime). Three parametric models proposed in the literature are compared and recalibrated, and a new model is proposed to account for the alternation of vertical atmosphere profiles by clouds. During the daytime, the proposed all-sky model has 15.3–31.8% lower

Table 8
LW modeling errors of original and calibrated all-sky models. Bold values indicate best performance.

		Daytime				Nighttime		All day	
Model	Eq. (23)	Eq. (24)	Eq. (25)	Eq. (26a)	Eq. (26b)	Eq. (23)	Eq. (26b)	Eq. (23)	Eq. (26b)
Original Coefficients	$c_1 = 1$ $c_2 = 1$ $c_3 = 1$ $c_4 = 1$	$c_1 = 0.273$ $c_2 = 0.809$	$c_1 = 1.202$ $c_2 = 0.303$	-	$c_1 = 1$ $c_2 = 1$ $c_3 = 1$ $c_4 = 1$	–	$c_1 = 1$ $c_2 = 1$ $c_3 = 1$ $c_4 = 1$	-	
MBE (W/m^2)	−2.89	−0.75	−36.55	–	–	0.31	–	−1.46	-
RMSE (W/m^2)	23.26	30.77	45.81	–	–	21.21	–	22.38	–
rMBE (%)	−0.86	−0.22	−10.93	–	–	0.1	–	−0.45	–
rRMSE (%)	6.96	9.2	13.71	–	–	6.78	–	6.93	–
Calibrated Coefficients	$c_1 = 0.48$ $c_2 = 0.89$ $c_3 = 0.57$ $c_4 = 0.92$	$c_1 = 0.23$ $c_2 = 1$	$c_1 = 1.2$ $c_2 = 0.17$	$c_1 = 1.29$ $c_2 = 0.8$ $c_3 = 0.7$ $c_4 = 0.78$ $c_5 = 0.13$	$c_1 = 0.96$ $c_2 = 1.2$ $c_3 = 0.49$ $c_4 = 1.09$ $c_5 = 0.15$	$c_1 = 0.82$ $c_2 = 1.13$ $c_3 = 0.83$ $c_4 = 1.11$	$c_1 = 0.77$ $c_2 = 0.8$ $c_3 = 0.39$ $c_4 = 0.8$ $c_5 = 0.16$	$c_1 = 0.82$ $c_2 = 1.24$ $c_3 = 0.83$ $c_4 = 1.21$	$c_1 = 0.78$ $c_2 = 1$ $c_3 = 0.38$ $c_4 = 0.95$ $c_5 = 0.17$
MBE (W/m^2)	−5.46	−11.4	−6.9	−3.09	−5.88	−2.57	−2.43	−4.94	−4.38
RMSE (W/m^2)	23.14	28.73	27.38	19.59	21.18	20.59	20.32	21.73	20.91
rMBE (%)	−1.63	−3.41	−2.06	−0.92	−1.76	−0.82	−0.78	−1.53	−1.35
rRMSE(%)	6.92	8.59	8.19	**5.86**	**6.34**	6.58	**6.49**	6.72	**6.47**

RMSE than the other three calibrated models. If GHI irradiance measurements are available, using CMF has 7.5% lower RMSE than using CF. During the nighttime and all day periods, the proposed model yields 1.3–3.8% lower RMSE than the recalibrated Crawford and Duchon model. For different applications that require LW information during daytime and/or nighttime, coefficients of the proposed model can be selected for use.

The main contributions of this work are: (1) We propose novel accurate parametric models to calculate 1-min averaged downward atmospheric longwave irradiance under both clear-sky and all-sky conditions. (2) The coefficients of the proposed models should be considered more universal, since data from seven climatologically diverse stations (rather than one or two particular locations) are used. (3) We also determined that several clear-sky parametric models proposed recently are equivalent.

Acknowledgments

The authors gratefully acknowledge the partial support by the California Energy Commission EPIC PON-13-303 program, which is managed by Dr. Silvia Palma-Rojas. The authors also thankful to Dr. Chi-Han Cheng from the University of Central Florida for downloading the ASOS cloud fraction data.

Appendix A

Adapted from Ref.Kasten and Young (1989); Ineichen and Perez (2002); Ineichen (2006); Ineichen (2008); Inman et al. (2015), the clear sky GHI is expressed as,

$$\mathrm{GHI}_c = c_1 I_0 \sin(\alpha_e) \cdot e^{0.01 m^{1.8} - c_2 m (f_1 + f_2 (T_L - 1))}$$

where c_1, c_2, f_1 and f_2 are altitude correction coefficients, I_0 (W/m^2) is the extraterrestrial irradiance, α_e (°) is the solar elevation angle, m is the air mass and T_L is the Linke turbidity factor. The clear sky DNI is expressed as,

$$\mathrm{DNI}_c = \left(0.664 + \frac{0.163}{f_1}\right) I_0 \cdot e^{-0.09 m (T_L - 1)}$$

The altitude correction coefficients are:

$$c_1 = 5.09 \times 10^{-5} \mathrm{Alt} + 0.868$$

$$c_2 = 3.92 \times 10^{-5} \mathrm{Alt} + 0.0387$$

$$f_1 = e^{-\mathrm{Alt}/8000}$$

$$f_2 = e^{-\mathrm{Alt}/1250}$$

with Alt (m) is the altitude. The extraterrestrial irradiance I_0 is expressed as,

$$I_0 = 1367.7\left(1 + 0.033 \cos\left(\frac{2\pi}{365.25}\mathrm{DOY}\right)\right)$$

with DOY is the day of year. The air mass m is expressed as a function of solar elevation angle,

$$\frac{1}{m} = \sin\alpha_e + 0.15\left(\alpha_e \frac{180}{\pi} + 3.885\right)^{-1.253}$$

The Linke turbidity factor T_L is extracted from monthly Link turbidity images. The above model can be used to calculated 1-min averaged clear-sky GHI and DNI.

References

Alados, I., Foyo-Moreno, I., Alados-Arboledas, L., 2012. Estimation of downwelling longwave irradiance under all-sky conditions. Int. J. Climatol. 32 (5), 781–793.
Alduchov, O.A., Eskridge, R.E., 1996. Improved Magnus form approximation of saturation vapor pressure. J. Appl. Meteorol. 35 (4), 601–609.
Berdahl, P., Fromberg, R., 1982. The thermal radiance of clear skies. Sol. Energy 29 (4), 299–314.
Berdahl, P., Martin, M., 1984. Emissivity of clear skies. Sol. Energy 32 (5), 663–664.
Bilbao, J., De Miguel, A.H., 2007. Estimation of daylight downward longwave atmospheric irradiance under clear-sky and all-sky conditions. J. Appl. Meteorol. Climatol. 46 (6), 878–889.
Brunt, D., 1932. Notes on radiation in the atmosphere. I. Quart. J. Roy. Meteorol. Soc. 58 (247), 389–420.
Brutsaert, W., 1975. On a derivable formula for long-wave radiation from clear skies. Water Resour. Res. 11 (5), 742–744.
Carmona, F., Rivas, R., Caselles, V., 2014. Estimation of daytime downward longwave radiation under clear and cloudy skies conditions over a sub-humid region. Theoret. Appl. Climatol. 115 (1–2), 281–295.
Crawford, T.M., Duchon, C.E., 1999. An improved parameterization for estimating effective atmospheric emissivity for use in calculating daytime downwelling longwave radiation. J. Appl. Meteorol. 38 (4), 474–480.
Dai, Q., Fang, X., 2014. A new model for atmospheric radiation under clear sky condition at various altitudes. Adv. Space Res. 54 (6), 1044–1048.
Dilley, A.C., O'brien, D.M., 1998. Estimating downward clear sky long-wave irradiance at the surface from screen temperature and precipitable water. Quart. J. Roy. Meteorol. Soc. 124 (549), 1391–1401.
Duarte, H.F., Dias, N.L., Maggiotto, S.R., 2006. Assessing daytime downward longwave radiation estimates for clear and cloudy skies in Southern Brazil. Agric. Forest Meteorol. 139 (3), 171–181.
Dupont, J.-C., Haeffelin, M., Drobinski, P., Besnard, T., 1984. Parametric model to estimate clear-sky longwave irradiance at the surface on the basis of vertical distribution of humidity and temperature. J. Geophys. Res.: Atmos. 113 (D7).
Eicker, U., Dalibard, A., 2011. Photovoltaic–thermal collectors for night radiative cooling of buildings. Sol. Energy 85 (7), 1322–1335.
Golden Gate Weather Service, 2016. El Niño and La Niña years and intensities. <http://ggweather.com/enso/oni.htm>.
Idso, S.B., 1981. A set of equations for full spectrum and 8-to 14-μm and 10.5-to 12.5-μm thermal radiation from cloudless skies. Water Resources Res. 17 (2), 295–304.
Idso, S.B., Jackson, R.D., 1969. Thermal radiation from the atmosphere. J. Geophys. Res. 74 (23), 5397–5403.
Ineichen, P., 2006. Comparison of eight clear sky broadband models against 16 independent data banks. Sol. Energy 80 (4), 468–478.
Ineichen, P., 2008. Conversion function between the linke turbidity and the atmospheric water vapor and aerosol content. Sol. Energy 82 (11), 1095–1097.
Ineichen, P., Perez, R., 2002. A new airmass independent formulation for the Linke turbidity coefficient. Sol. Energy 73 (3), 151–157.
Inman, R.H., Edson, J.G., Coimbra, C.F.M., 2015. Impact of local broadband turbidity estimation on forecasting of clear sky direct normal irradiance. Sol. Energy 117, 125–138.
Iowa State University of Science and Technology, 2016. ASOS-AWOS-METAR data download. <https://mesonet.agron.iastate.edu/request/download.phtml>.
Iziomon, M.G., Mayer, H., Matzarakis, A., 2003. Downward atmospheric longwave irradiance under clear and cloudy skies: measurement and parameterization. J. Atmos. Sol. Terr. Phys. 65 (10), 1107–1116.
Kasten, F., Young, A.T., 1989. Revised optical air mass tables and approximation formula. Appl. Opt. 28 (22), 4735–4738.
Konzelmann, T., van de Wal, R.S., Greuell, W., Bintanja, R., Henneken, E.A., Abe-Ouchi, A., 1994. Parameterization of global and longwave incoming radiation for the Greenland Ice Sheet. Global Planet. Change 9 (1), 143–164.
Maghrabi, A., Clay, R., 2011. Nocturnal infrared clear sky temperatures correlated with screen temperatures and GPS-derived PWV in Southern Australia. Energy Convers. Manage. 52 (8), 2925–2936.
Mills, A.F., Coimbra, C.F.M., 2015. Basic Heat and Mass Transfer. Temporal Publishing, San Diego, CA.
National Oceanic and Atmospheric Administration, 1998. Automated surface observing system user's guide. <http://www.nws.noaa.gov/asos/pdfs/aum-toc.pdf>.
National Oceanic and Atmospheric Administration, 2015. SURFRAD Network. <http://www.esrl.noaa.gov/gmd/grad/surfrad/>.
Niemelä, S., Räisänen, P., Savijärvi, H., 2001. Comparison of surface radiative flux parameterizations: Part I: Longwave radiation. Atmos. Res. 58 (1), 1–18.
Prata, A.J., 1996. A new long-wave formula for estimating downward clear-sky radiation at the surface. Quart. J. Roy. Meteorol. Soc. 122 (533), 1127–1151.
Reno, M.J., Hansen, C.W., Stein, J.S., 2012. Global horizontal irradiance clear sky models: implementation and analysis, SANDIA report SAND2012-2389.
Ruckstuhl, C., Philipona, R., Morland, J., Ohmura, A., 1984. Observed relationship between surface specific humidity, integrated water vapor, and longwave downward radiation at different altitudes. J. Geophys. Res.: Atmos. 112 (D3).
Satterlund, D.R., 1979. An improved equation for estimating long-wave radiation from the atmosphere. Water Resour. Res. 15 (6), 1649–1650.
Swinbank, W.C., 1963. Long-wave radiation from clear skies. Quart. J. Roy. Meteorol. Soc. 89 (381), 339–348.
Tang, R., Etzion, Y., Meir, I.A., 2004. Estimates of clear night sky emissivity in the Negev Highlands, Israel. Energy Convers. Manage. 45 (11), 1831–1843.
Zaversky, F., García-Barberena, J., Sánchez, M., Astrain, D., 2013. Transient molten salt two-tank thermal storage modeling for CSP performance simulations. Sol. Energy 93, 294–311.